Nanometre-scale rolling and sliding of carbon nanotubes

M. R. Falvo*†, R. M. Taylor II†‡, A. Helser‡, V. Chi‡, F. P. Brooks Jr‡, S. Washburn*† & R. Superfine*†

*Departments of * Physics and Astronomy, and ‡ Computer Science, † North Carolina Center for Nanoscale Materials, University of North Carolina, Chapel Hill, North Carolina 27599, USA*

Understanding the relative motion of objects in contact is essential for controlling macroscopic lubrication and adhesion, for comprehending biological macromolecular interfaces, and for developing submicrometre-scale electromechanical devices[1,2]. An object undergoing lateral motion while in contact with a second object can either roll or slide. The resulting energy loss and mechanical wear depend largely on which mode of motion occurs. At the macroscopic scale, rolling[3] is preferred over sliding, and it is expected to have an equally important role in the microscopic domain. Although progress has been made in our understanding of the dynamics of sliding at the atomic level[4], we have no comparable insight into rolling owing to a lack of experimental data on microscopic length scales. Here we produce controlled rolling of carbon nanotubes on graphite surfaces using an atomic force microscope. We measure the accompanying energy loss and compare this with sliding. Moreover, by reproducibly rolling a nanotube to expose different faces to the substrate and to an external probe, we are able to study the object over its complete surface.

The microscopic aspects of tribology have been explored by means of the surface force apparatus (SFA)[5] and atomic force microscopy (AFM)[6], which have identified the intrinsic dependence of sliding friction on contact area[7,8] and crystallographic orientation[9,10]. Further, AFM has been used to perform friction mapping of surfaces with atomic resolution[4] and has identified stick–slip motion in the sliding of nanometre-scale objects[11]. Using AFM manipulation[12,13] of multiwall carbon nanotubes (CNTs), we have observed sliding and rolling. CNTs, with a range of available sizes down to the molecular scale, serve as interesting model systems for tribological studies. In addition, nanotubes are expected to play a part in future nanometre-scale electrical-mechanical devices, and rolling fullerenes have been proposed as ideal lubricants[14–16]. Our evidence for sliding and rolling comprises sequences of topographical images of manipulated nanotubes and lateral force data acquired during the manipulation to measure energy loss.

Samples were prepared by solvent evaporation on mica and graphite substrates from an ethanol solution of raw carbon soot produced by the carbon arc technique[17]. The multiwall CNTs were imaged and manipulated under ambient conditions. The nanomanipulator AFM system[18,19], designed for manipulation, comprises an advanced visual interface, teleoperation capabilities for manual control of the AFM tip and haptic (touch) presentation of the AFM data (Topometrix Discoverer). Normal force, lateral force and AFM tip trajectory are recorded simultaneously for strict correlation. The AFM tip is used to apply lateral forces at locations along the tube to produce translations and rotations. These tubes are free of pinning material and move without deformation. The lateral force values have been calibrated from measured cantilever and tip geometry, literature values for the cantilever (Si) elastic moduli and the detector response from the *z*-translation of the cantilever. We estimate the absolute error in this calibration to be about 30%, with the largest contribution in the uncertainty coming from the AFM tip geometry.

We first summarize our results for manipulation on mica and graphite, then focus on the results relevant to rolling. An extended object such as a CNT can be pushed from the end or from the side, with possible outcomes including sliding, rolling or some combination of both. On mica, end-on pushes produce a single, pronounced initial stick–slip peak in the lateral force trace which is absent in side-on pushes. Side-on pushes produce no stick–slip features and are accompanied by an in-plane rotation of the nanotube. On graphite, end-on pushes show a series of stick–slip peaks. However, side-on pushes on graphite reveal new behaviour. In addition to cases where a relatively smooth lateral force trace is accompanied by an in-plane rotation (sliding), we also observe cases where the CNT has a pronounced, periodic, stick–slip modulation. In this case, which we refer to as rolling, the tube undergoes no in-plane

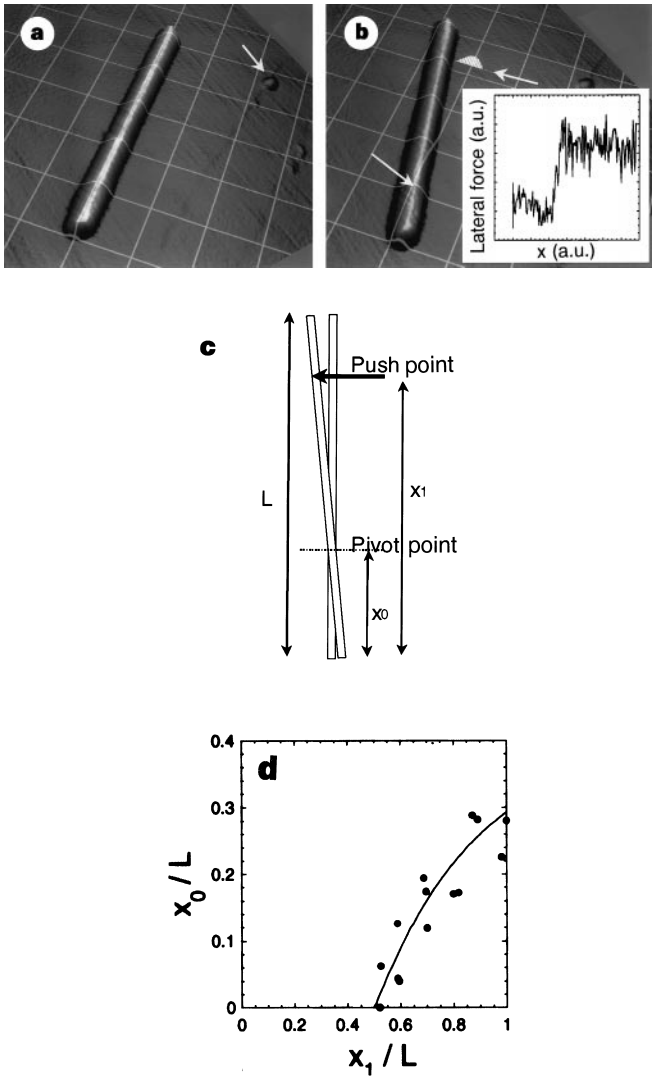

Figure 1 Sliding carbon nanotube. **a**, The tube lies in its original position. Grid lines are overlain so that one of the grid axes corresponds to the original orientation of the tube axis. The absolute position of the grid relative the fiducial feature indicated by the arrow was adjusted to be consistent with that in **b** so that the point of rotation could be determined. **b**, The tube's orientation after AFM manipulation. The pivot point and push point are indicated by the bottom and top arrows, respectively. The white dashes to the right of the push point are markers indicating the trajectory of the AFM tip during manipulation. Inset shows the lateral force trace during a sliding manipulation. The step height is approximately ten times smaller than the stick peaks shown in Fig. 2g. **c**, Diagram of the pushing process. Measuring from the bottom of the tube, x_1 is the push point, and x_0 is the point of rotation (or pivot point). **d**, The relation between the push point and the pivot point for several pushing trials is compared with equation (1) in the text, with no fitting parameters (plotted as a solid curve).

rotation, and the topographical data change in an appropriate fashion for roll-wise reorientation.

We describe the sliding case first. When the nanotube is manipulated from the side on mica or graphite, one class of outcomes features a relatively smooth lateral force jump (inset in Fig. 1b). These manipulations are accompanied by an in-plane rotation of the CNT about a pivot point that depends on the location of the AFM tip during the push. This dependence is shown in Fig. 1, where the AFM images show the position of the AFM tip during the push of a nanotube on graphite, and the overlay of a measuring grid used to determine the tube rotation and the pivot point. A unique relation between the point of manipulation and the point of rotation can be derived with no fitting parameters[20] by solving for the motion that minimizes the energy loss due to friction. Uniform friction is assumed, and only sliding/in-plane rotation about an axis perpendicular to the surface is considered. The normalized pivot point location, $x_0' = x_1/L$, to obtain

$$x_0' = x_1' - \sqrt{x_1'^2 - \frac{1}{2}(2x_1' - 1)} \qquad (1)$$

which is compared to the measurements in the inset to Fig. 1b. This approach is easily generalized to other object shapes. This result suggests that the friction between the CNT cylinder and graphite substrate is uniform along the tube and strongly favours the interpretation of the nanotube motion as sliding. If the nanotube were rolling, the sliding friction at the tube/substrate contact would vary along the length of the tube. We note that this result indicates predictability in the manipulation of nanometer-scale objects, and foreshadows robotic assembly of surface-bound structures[21,22].

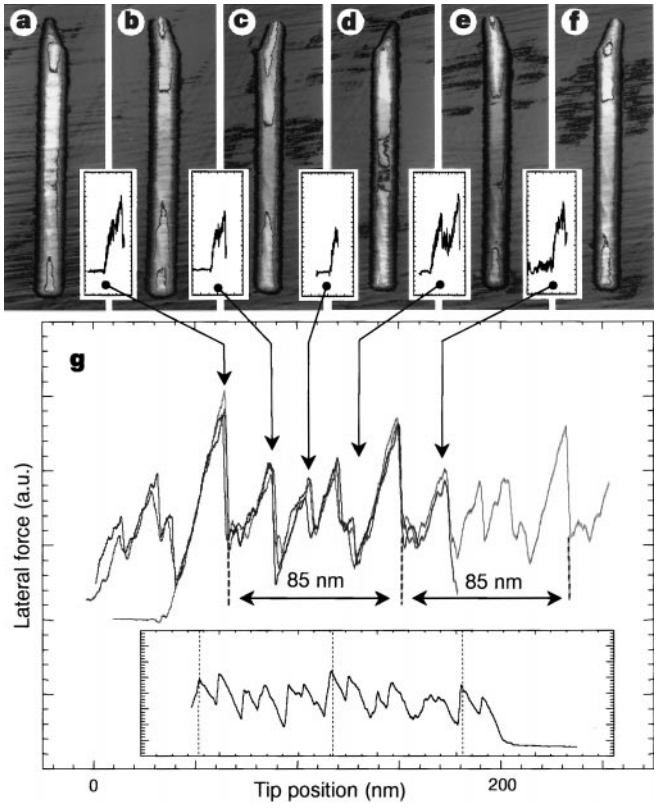

Figure 2 Rolling carbon nanotube. **a–f**, The tube as it is manipulated from left to right. The tube is imaged before and after each of the 5 manipulations. The insets between each topographical image show the lateral force during each manipulation. The tube is moving from left to right not gradually, but in sudden slips in a stick-slip type rolling motion. In **g**, three overlapped signals from separate rolling trials are shown for the lateral force as the tube is pushed through several revolutions of stick-slip rolling motion. The features of the force traces are remarkably reproducible. The 85 nm periodicity in the signal, indicated by the dashed lines, is equal to the circumference of the tube at its ends. A signal for a push in the opposite direction is shown in the inset at the bottom of **g**. This signal differs in form but also has a reproducible 85 nm periodicity. Stick-slip phenomena are known to be hysteretic, explaining the lack of correspondence in the details of the forward and reverse traces.

Most dramatic is the rolling behaviour discovered in the manipulation of large nanotubes from the side-on graphite substrates. In these cases, we have observed changes in nanotube topography correlated with both lateral force stick-slip and the absence of in-plane rotation. The stick–slip signatures in the lateral force data for manipulations in either direction show a periodicity corresponding to the nanotube circumference (Fig. 2g) and are reproducible in detail. The CNT of Fig. 2 (tube A) is 500 nm long and has an average radius at the ends of 13.3 nm and at mid-length of 8.5 nm. The period of the lateral force signals in either direction is 85 ± 2 nm, corresponding to the tube circumference, 83 ± 3 nm. A stick–slip type motion causes the sawtooth shape of these signals. The tip is deflected up to a threshold lateral force and a slip–roll occurs, undeflecting the cantilever. To confirm the stick–slip motion, we performed gradual pushes in which the tip was slowly moved against the CNT while monitoring the lateral force. When the tip was pushed so that the lateral force increased but was turned around before a sudden decrease in the signal (no slip), the subsequently acquired topographical data indicated no resultant movement of the CNT.

The stick–slip peaks were used to reorient reproducibly the CNT on the surface. If the application of the AFM tip was stopped just after a stick-peak, the subsequently acquired topography image showed that the CNT had rotated a fixed amount. The insets between topographs in Fig. 2 show lateral force traces for the pushes between the particular orientations. The change in the tube-end shape from image to image indicates a rolling reorientation. Note that in Fig. 2b, e and 2c, f, tube-end shapes are similar, indicating a similar rolling orientation. In addition to the tube-end shape, the topographical data indicates linear translation between images, which is consistent with a rolling-without-slipping motion. Particularly notable is the upper end of the tube, which has a conical cap consistent with examples identified by transmission electron microscopy[23]. A set of data such as these, taken from several sides, can be assembled to provide a three-dimensional reconstruction of a complex object.

The combination of topographical and lateral force data indicates that this tube is undergoing stick–slip rolling motion. There are two important questions. What is the origin of stick–slip in rolling? And what determines whether rolling or sliding will occur in any given translation? The direct correspondence between lateral force features and the nanotube topography implies that adhesion hysteresis is the dominant energy loss mechanism and is responsible for the stick–slip dynamics. A peeling mechanism for the resistance to rolling has been observed for macroscopic rolling experiments[24]. For example, the amplitudes of the individual stick–slip peaks should be correlated with the varying contact area of the structured tube over the course of its roll. The amplitudes of these peaks can be placed into the context of the van der Waals adhesion of the nanotube at the surface. We can estimate the adhesion force using the van der Waals attraction for the cylinder-on-flat geometry[5] for a tube (tube B) for which we have taken calibrated lateral force data in rolling. For tube B ($R = 13.5$ nm, $L = 590$ nm) we calculate an adhesive force of 800 nN. This calculation assumes a distance between tube and surface equal to the interlayer spacing in graphite (0.34 nm) and assumes no intervening medium. This force, which completely separates the tube from the substrate, should represent an upper bound for the force required for rolling. In fact, our rolling stick–slip peaks fall well below this value, in the range 20–50 nN.

We can compare our measurements of the sliding friction for a variety of nanotubes by using a simple model for the force due to friction, given by $F = swL$, where s is the interfacial shear stress, w is

the contact width, and L is the nanotube length. These quantities are difficult to measure independently and calculations are model-dependent. As a guide, we apply a *JKR* model for the contact of cylinders[25] and find a contact width of 3 nm for a tube radius of 13.5 nm. Our measurements of 0.006 N m^{-1} for the friction force per unit length is then consistent with a shear stress of 2×10^6 Pa. This can be compared with a value of 5×10^6 Pa, as inferred from AFM tip/graphite measurements[16]. To compare rolling and sliding in a single tube, we can calculate the force (4 nN for $L = 590$ nm) and that would be needed to slide tube B, which in fact rolls. Finally, we note that the area under the lateral force trace is a direct measure of energy loss in rolling. For tube B, we measure an energy loss of $(8 \pm 3) \times 10^{-16}$ J per revolution. The sliding energy loss expected for this distance (85 nm) can be calculated using the frictional force of 4 nN, yielding 3×10^{-16} J.

When we compare our lateral force measurements for sliding and rolling cases, we find that the stick peaks in rolling are higher than the lateral force needed to sustain sliding, and that the energy cost for rolling is larger than that of the sliding cases. Why should the nanotubes roll? We speculate that, owing to the size and surface features of the rolling nanotubes, a stick peak for sliding in side-on pushing might exist that is larger than the threshold for rolling. Atomic-scale substrate interactions may also play a roll as we have observed this characteristic rolling only on graphite. Rolling behaviour has been accompanied by a preferential, threefold, in-plane orientation that indicates intimate nanotube/graphite contact, and perhaps lattice registry. Rolling may occur only when both the nanotube and the underlying graphite have long-range order. In these cases that there may be a barrier for sliding which is larger than that for rolling and may preclude the direct measurement of sliding friction[7]. □

Received 27 July; accepted 10 September 1998.

1. Persson, B. N. J. *Sliding Friction: Physical Properties and Applications* (Springer, Berlin, 1998).
2. Bhushan, B., Israelachvili, J. N. & Landman, U. Nanotribology: friction, wear and lubrication at the atomic scale. *Nature* **374,** 607–616 (1995).
3. Johnson, K. L. *Contact Mechanics* (Cambridge University Press, New York, 1994).
4. Mate, M. C., McClelland, G. M., Erlandsson, R. & Chiang, S. Atomic-scale friction of a tungsten tip on a graphite surface. *Phys. Rev. Lett.* **59,** 1942–1945 (1987).
5. Israelachvili, J. *Intermolecular and Surface Forces* (Academic, San Diego, 1991).
6. Binnig, G., Quate, C. F. & Gerbre, C. Atomic force microscope. *Phys. Rev. Lett.* **56,** 930–933 (1986).
7. Sheehan, P. E. & Lieber, C. M. Nanotribology and nanofabrication of MoO_3 structures by atomic force microscopy. *Science* **272,** 1158–1161 (1996).
8. Johnson, K. L. in *Micro/nanotribology and its Applications* (ed. Bhushan, B.) 157 (Kluwer Academic, Dordrecht, The Netherlands, 1997).
9. Hirano, H., Shinjo, K., Kaneko, R. & Murata, Y. Anisotropy of frictional forces in muscovite mica. *Phys. Rev. Lett.* **67,** 2642–2645 (1991).
10. Overney, R. M., Takano, H., Fujihira, M., Paulus, W. & Ringsdorf, H. Anisotropy in friction and molecular stick–slip motion. *Phys. Rev. Lett.* **72,** 3546–3549 (1994).
11. Luthi, R. *et al.* Sled-type motion on the nanometer scale: Determination of dissipation and cohesive energies of C_{60}. *Science* **266,** 1979–1981 (1994).
12. Falvo, M. R. *et al.* Bending and buckling of carbon nanotubes under large strain. *Nature* **389,** 582–584 (1997).
13. Hertel, T., Martel, R. & Avouris, P. Manipulation of individual carbon nanotubes and their interactions with surfaces. *J. Phys. Chem. B* **102,** 910–915 (1998).
14. Rapoport, L. *et al.* Hollow nanoparticles of WS2 as potential solid-state lubricants. *Nature* **387,** 791–793 (1997).
15. Bhushan, B., Gupta, B. K., Van Cleef, G. W., Capp, C. & Coe, J. V. Sublimed C^{60} films for tribology. *Appl. Phys. Lett.* **62,** 3253–3255 (1993).
16. Schwarz, U. D., Zworner, O., Koster, P. & Wiesendanger, R. Quantitative analysis of the frictional properties of solid materials at low loads. 1. Carbon compounds. *Phys. Rev. B* **56,** 6987–6996 (1997).
17. Ebbesen, T. W. & Ajayan, P. M. Large-scale synthesis of carbon nanotubes. *Nature* **358,** 220–222 (1992).
18. Taylor, R. M. *et al. SIGGRAPH '93* (ACM SIGGRAPH, New York, 1993).
19. Finch, M. *et al. ACM Symposium on Interactive 3D Graphics* (ACM SIGGRAPH, Monterey, California, 1995).
20. Prescott, J. *Mechanics of Particles and Rigid Bodies* (Longmans, Green and Co., London, 1936).
21. Baur, C. *et al.* Robotic nanomanipulation with a scanning probe microscope in a networked computing environment. *J. Vac. Sci. Tech. B* **15,** 1577–1580 (1997).
22. Mason, M. T. & Salisbury, J. K. J. *Robot Hands and the Mechanics of Manipulation* (MIT Press, Cambridge, Massachusetts, 1985).
23. Ebbesen, T. W. & Takada, T. Topological and sp^3 defect structures in nanotubes. *Carbon* **33,** 973–978 (1995).
24. Kendall, K. Rolling friction and adhesion between smooth solids. *Wear* **33,** 351–358 (1975).
25. Chaudhury, M. J., Weaver, T., Hui, C. Y. & Kramer, E. J. Adhesive contact of cylindrical lens and a flat sheet. *J. Appl. Phys.* **80,** 30–37 (1996).

Acknowledgements. We thank O. Zhou for CNT soot material, S. Paulson for helping to solve sample-preparation problems, and the entire Nanomanipulator team. The NSF, the NIH, the Office of Naval Research, and Topometrix Inc. provided financial support for this work.

Correspondence and requests for materials should be addressed to R.S. (e-mail: rsuper@physics.unc.edu).

Identifying the forces responsible for self-organization of nanostructures at crystal surfaces

K. Pohl*, M. C. Bartelt*, J. de la Figuera*, N. C. Bartelt*, J. Hrbek*† & R. Q. Hwang*

* *Sandia National Laboratories, Livermore, California 94550, USA*

The spontaneous formation of organized surface structures at nanometre scales[1,2] has the potential to augment or surpass standard materials patterning technologies. Many observations of self-organization of nanoscale clusters at surfaces have been reported[1–10], but the fundamental mechanisms underlying such behaviour—and in particular, the nature of the forces leading to and stabilizing self-organization—are not well understood. The forces between the many-atom units in these structures, with characteristic dimensions of one to tens of nanometres, must extend far beyond the range of typical interatomic interactions. One commonly accepted source of such mesoscale forces is the stress field in the substrate around each unit[1,11–13]. This, however, has not been confirmed, nor have such interactions been measured directly. Here we identify and measure the ordering forces in a nearly perfect triangular lattice of nanometre-sized vacancy islands that forms when a single monolayer of silver on the ruthenium (0001) surface is exposed to sulphur at room temperature. By using time-resolved scanning tunnelling microscopy to monitor the thermal fluctuations of the centres of mass of the vacancy islands around their final positions in the self-organized lattice, we obtain the elastic constants of the lattice and show that the weak forces responsible for its stability can be quantified. Our results are consistent with general theories of strain-mediated interactions between surface defects in strained films.

We began by depositing slightly less than one monolayer (ML) of Ag at room temperature on a clean Ru(0001) surface prepared in ultrahigh vacuum. A Ag film forms that is highly strained as a result of the ~7% lattice mismatch between Ag and Ru. A flash anneal to 750 K, to obtain an equilibrium Ag film, one single layer high, invariably produces an ordered pattern in the film (unit cell $\sim 40 \times 60$ Å) consisting of a near-square array of threading dislocations[14,15]. Subsequent exposure of this strained layer to sulphur, at room temperature, triggers strikingly complex behaviour in the Ag film, as sulphur displaces Ag atoms. Here we describe two main regimes distinguished by the sulphur coverage, θ_S.

For low $\theta_S < 0.05$ ML, scanning tunnelling microscopy (STM) images show far-separated two-dimensional vacancy islands of highly regular size, about 34 ± 11 Å diameter (Fig. 1a, b). Sulphur is found coating exposed Ru regions, including the inside of the islands where it forms ordered two-dimensional clusters (Fig. 1b inset). This is not surprising because the interaction of sulphur with Ru is considerably stronger than that with Ag, and it certainly reduces the energy cost of exposing the Ru(0001) surface by decreasing its surface energy.

The isolated vacancy islands are extremely mobile (Fig. 1a, b), significantly more so than has been reported for vacancy islands of similar size on clean metal (111) surfaces[16,17]. Islands diffuse perhaps by atoms diffusing along the edges of islands, although other mechanisms involving a flow of atoms across an island, or exchange of edge atoms with the sulphur and Ag adatom gas, could also be significant. We measured island hop rates of several hundreds of

† Permanent address: Brookhaven National Laboratory, Upton, New York 11973, USA